*Stanford Exploration Project, Report 120, May 3, 2005, pages 1–23*

# 3-D subsalt imaging via regularized inversion with model preconditioning

*Marie L. Clapp and Robert G. Clapp*[1]

**ABSTRACT**

Subsalt imaging is a difficult but increasingly important problem. The poor illumination that occurs when seismic energy is affected by the complex subsurface at and around salt bodies causes significant shadow zones in migration results. These shadow zones may contain real signal, but it is weak compared to the artifacts caused by multipathing and poor illumination. To reduce artifacts and recover this energy, thereby improving the image, we use an imaging (migration) operator in a regularized least-squares inversion. The regularization operator acts on the offset ray parameter (reflection angle) axis of the model space. Performing several iterations of regularized inversion that penalize large changes along the offset ray parameter axis results in an image with recognizable events in the shadow zones and fewer artifacts. We perform regularized inversion with model preconditioning on real 2-D and 3-D data to obtain seismic images that are better in poorly illuminated areas than migration results.

## INTRODUCTION

Our ongoing quest for hydrocarbons requires that we improve our ability to image the earth's subsurface. This is particularly true in areas around salt bodies, which can be good hydrocarbon traps but cause poor seismic illumination in the surrounding subsurface. Conventional imaging techniques such as migration cannot provide an adequate picture of these poorly illuminated areas (Muerdter et al., 1996; Prucha et al., 1998). In such areas, random noise and processing artifacts can easily obscure the small amount of signal that exists. A common type of artifact seen in these areas is caused by multipathing. Many authors have reduced these artifacts by generating images through Kirchhoff-type migration that create angle domain common image gathers (Xu et al., 2001). The artifacts are even better handled by downward-continuation migration (Prucha et al., 1999a; Stolk and Symes, 2004). However, reducing multipathing artifacts does not significantly improve the image where illumination is poor. To create improvements, we will have to deal with both these artifacts and the poor illumination which means we must move beyond migration.

Although migration is not sufficient to image the subsurface in areas with poor illumination, we can use migration as an imaging operator in a least-squares inversion scheme (Nemeth

[1]**email:** marie@sep.stanford.edu, bob@sep.stanford.edu

et al., 1999; Duquet and Marfurt, 1999; Ronen and Liner, 2000). In areas with poor illumination, the inversion problem is ill-conditioned, therefore it is wise to regularize the inversion scheme (Tikhonov and Arsenin, 1977). The regularization operator can be designed to exploit knowledge we have about the expected amplitude behavior and dip orientation of events in the image (Prucha and Biondi, 2002).

When using regularized inversion for imaging, the choice of regularization operator is critical. If it were possible for the subsurface to be perfectly illuminated, we would expect the amplitudes of the seismic events to vary smoothly with reflection angle. THerefore, an intelligent and fairly safe choice of regularization is to penalize large amplitude changes as the reflection angle varies for a given point in the subsurface (Kuehl and Sacchi, 2001; Prucha and Biondi, 2002). We refer to this as "geophysical" regularization. This process will help to reduce artifacts and improve the image.

In this paper, we examine the effects of geophysically regularized inversion on a real 3-D dataset. We will begin by explaining the basic theory of regularized inversion with model preconditioning (RIP). We will then demonstrate its use on a real 2-D line and the real 3-D volume that the 2-D line is taken from.

## BASIC THEORY

Our inversion scheme is based on the downward-continuation migration explained by Prucha et al. (1999a). To summarize, this migration is carried out by downward continuing the wavefield in frequency space, slant stacking at each depth, and extracting the image at zero time. The result is an image in depth (z), space (x and y), and offset ray parameter ($p_h$). Offset ray parameter is related to the reflection angle ($\theta$) and the dip angle of the reflector ($\phi$) in 2-D as:

$$\frac{\partial t}{\partial h} = p_h = \frac{2 \sin\theta \cos\phi}{V(z,x)}. \tag{1}$$

In complex areas, the image produced by downward-continuation migration will suffer from poor illumination. To compensate for this, we use the migration as an operator in a least-squares inversion. The inversion procedure used in this paper can be expressed as fitting goals as follows:

$$\begin{aligned} \mathbf{0} &\approx \mathbf{Lm} - \mathbf{d} \\ \mathbf{0} &\approx \epsilon \mathbf{Am}. \end{aligned} \tag{2}$$

The first equation is the "data fitting goal," meaning that it is responsible for making a model that is consistent with the data. The second equation is the "model styling goal," meaning that it allows us to impose some idea of what the model should look like using the regularization operator **A**. The model styling goal also helps to prevent a divergent result.

In the data fitting goal, **d** is the input data and **m** is the image obtained through inversion. **L** is a linear operator, in this case it is the adjoint of the downward-continuation migration scheme summarized above and explained by Prucha et al. (1999b). In the model styling goal, **A** is a regularization operator and $\epsilon$ controls the strength of the regularization.

Unfortunately, the inversion process described by fitting goals (2) can take many iterations to produce a satisfactory result. We can reduce the necessary number of iterations by making the problem a preconditioned one. We use the preconditioning transformation $\mathbf{m} = \mathbf{A}^{-1}\mathbf{p}$ (Fomel et al., 1997; Fomel and Claerbout, 2003) to give us the following fitting goals:

$$\begin{aligned} \mathbf{0} &\approx \mathbf{L}\mathbf{A}^{-1}\mathbf{p} - \mathbf{d} \\ \mathbf{0} &\approx \epsilon\mathbf{p}. \end{aligned} \tag{3}$$

$\mathbf{A}^{-1}$ is obtained by mapping the multi-dimensional regularization operator **A** to helical space and applying polynomial division (Claerbout, 1998). We call this least-squares minimization scheme Regularized Inversion with model Preconditioning (RIP).

The question now is what the regularization operator **A** is. In this paper, we will use geophysical regularization, which acts horizontally along the offset ray parameter axis (Clapp, 2003). It is designed to penalize sudden large changes in amplitudes, such as those caused by poor illumination.

## THE DATASET

The dataset upon which we have chosen to demonstrate RIP is a subset of the real 3-D Gulf of Mexico dataset provided to SEP by BP and ExxonMobil. The portion of the 3-D velocity model for the subset we are using can be seen in Figure 1. This subset contains 600 inline positions and 72 crossline positions. The salt body on the right side causes significant shadow zones that may mask potential hydrocarbon reservoirs. There are known 3-D faults in the sediments away from the salt and it is likely that more faults exist beneath salt in the shadow zones. The velocity model is believed to be accurate, which is important given the nature of our geophysical regularization operator.

## 2-D RESULTS

To test RIP on a real 2-D example, we extracted a single line from the subset of the deep water Gulf of Mexico dataset. This line is located at the crossline position of 20 km, chosen in an attempt to minimize the 3-D effects of the salt structure. However, this line will still be affected by the 3-D faults known to run through this volume.

Recall that the regularization operator used for geophysical RIP acts along the offset ray parameter axis. The strength of regularization (see the fitting goals (3)) for this real data example, $\epsilon = .001$, was chosen by trial and error. We have chosen to display the results after

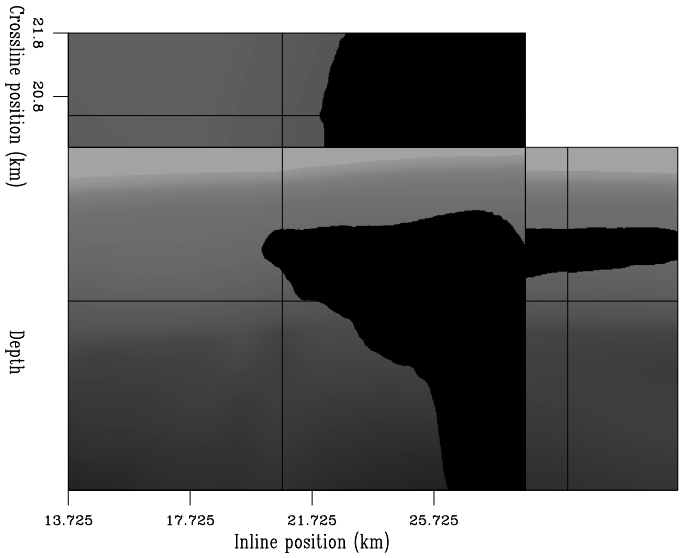


Figure 1: Subset of the BP Gulf of Mexico velocity model. marie1-bpvel [CR]

6 iterations which was selected based on data space residuals, as will be explained later. The result can be seen in Figure 2. The migration result is displayed above the geophysical RIP result. Both show a common ray parameter section on the left and a common image gather (CIG) on the right. The vertical lines indicate which common reflection point (CRP) location and offset ray parameter value the panels are taken from. The effect of the regularization is clearest in the CIG. The common ray parameter section also shows the effects. The result shows a crisper image after RIP, with fewer artifacts. To see the improvements more clearly, we have zoomed in on the area beneath the salt in Figure 3.

In Figure 3, the same ovals are shown on the migration result (top) and the geophysical RIP result (bottom). It is particularly clear that the holes in the common image gather are being filled by RIP. The whole common ray parameter section is cleaner than the one from the migration result. The subsalt reflectors are extending into the shadow zones everywhere, particularly in the areas indicated by the ovals. Geophysical RIP produces a cleaner result with better illumination than migration.

It is also interesting to stack the results (Figure 4). Once again, the stack of the migration result is shown on top and the stack of the result after 6 iterations of geophysical RIP is on the bottom. The ovals indicate where the reflectors extend farther into the shadow zones. In the RIP result, some reflectors can be seen almost all the way through the poorly illuminated areas. Also, the artifacts seen in the stack of the migration result are reduced in the RIP result.

As mentioned earlier, we chose to display the RIP results after 6 iterations based on an examination of the data space residuals as the least-squares inversion was performed. The data space residuals for each iteration can be seen in Figure 5. Each row is a collection of CMP gathers taken from locations across the whole survey. We have taken the envelope of the energy and clipped the high values, which appear as solid black regions. The first row is the original data, the second row shows the same CMP gathers after 2 iterations, the third row is after 4 iterations, fourth row after 6 iterations, fifth row after 8 iterations and sixth after 10

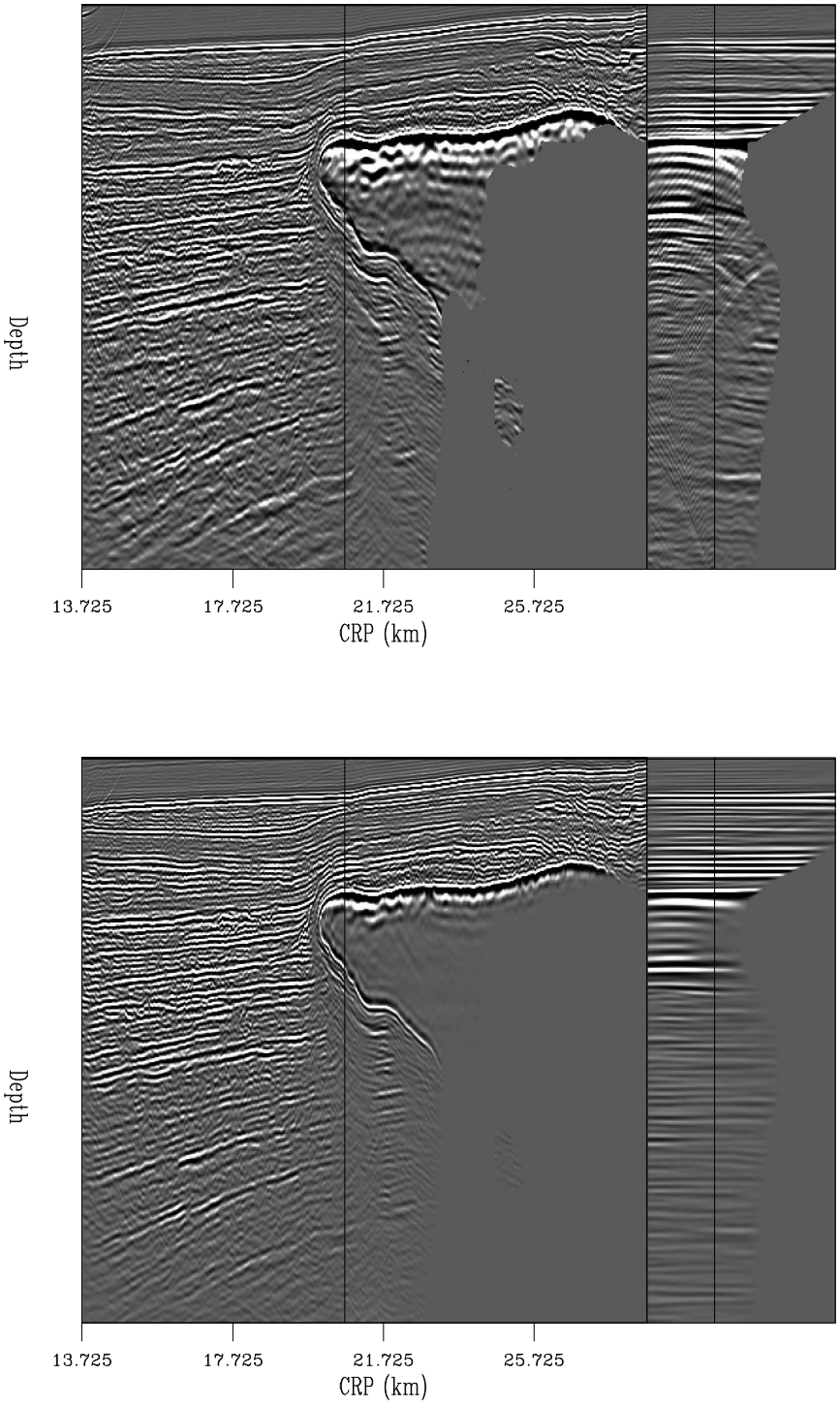


Figure 2: Top: result of downward-continuation migration of 2-D line. Left part is a common offset ray parameter section at $p_h = .265$, right part is a common image gather from $CRP = 20.675$. Bottom: result of 6 iterations of geophysical RIP. marie1-bp2d.1 [CR,M]

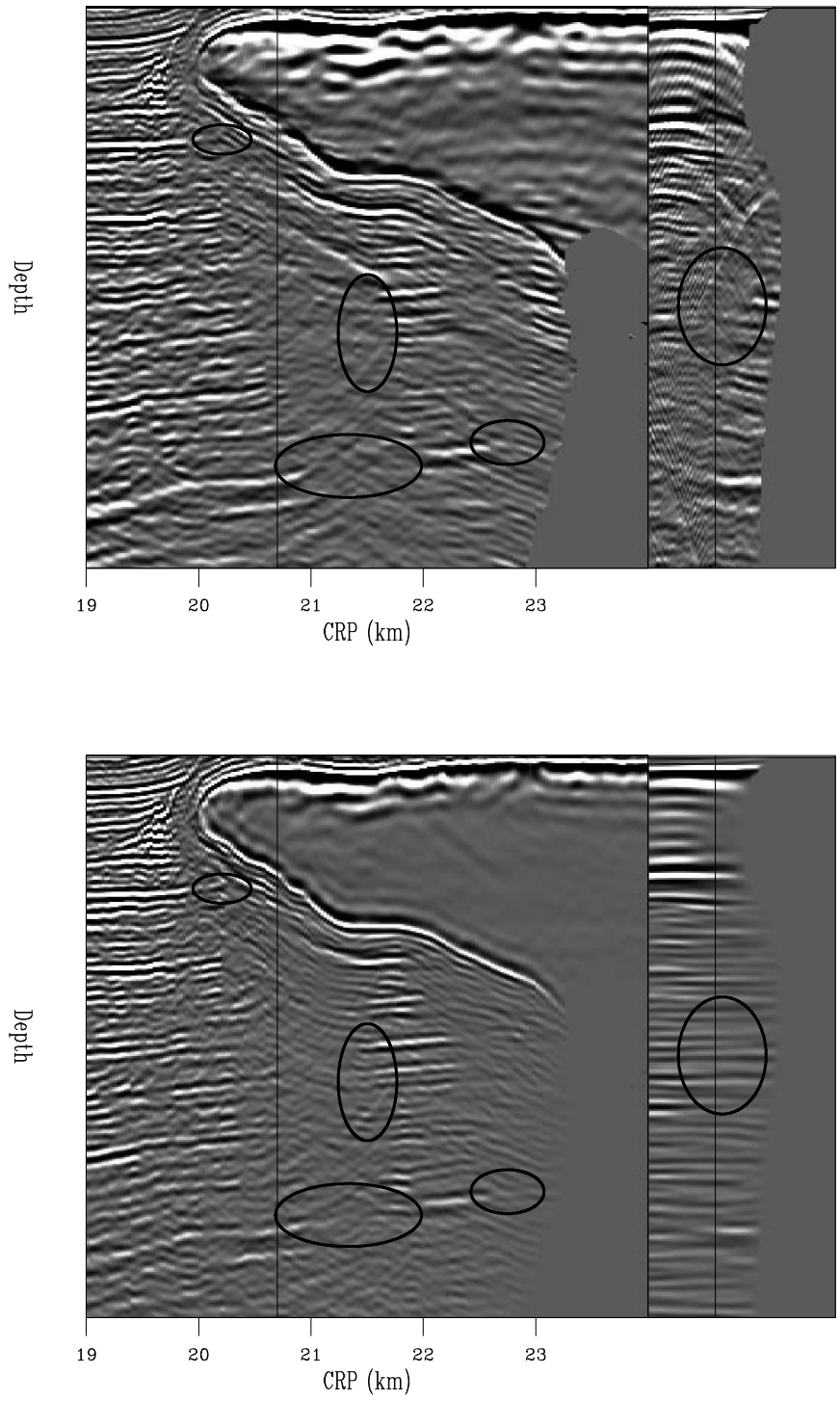


Figure 3: Zoomed portion of Figure 2. Top: result of downward-continuation migration of 2-D line. Left part is a common offset ray parameter section at $p_h = .265$, right part is a common image gather from $CRP = 20.675$. Bottom: result of 6 iterations of geophysical RIP. Ovals indicate areas where poor illumination exists in the migration result and is improved in the RIP result. marie1-zbp2d.1 [CR,M]

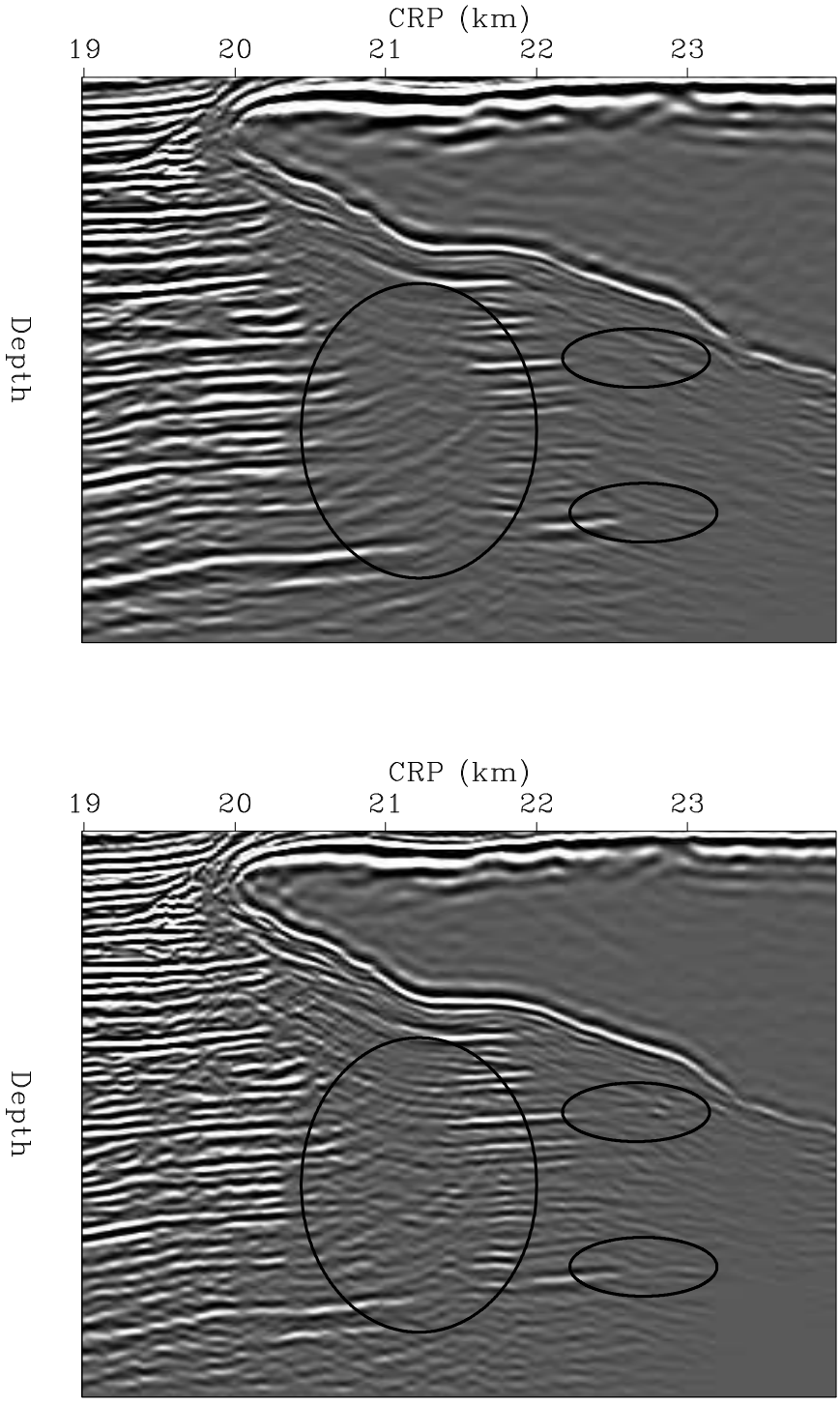


Figure 4: Top: stack of the result of downward-continuation migration of 2-D line. Bottom: stack of the result of 6 iterations of geophysical RIP. Ovals indicate areas where poor illumination exists in the migration result and is improved in the RIP result. marie1-zstackbp2d [CR,M]

iterations. The salt body begins at a CMP location between the fifth and sixth gathers shown in each row.

The biggest change in the residual energy occurs within the first two iterations, as would be expected. We see that the residual energy away from the salt decreases quickly (the black areas decrease). The residual energy associated with the salt also decreases, with the exception of energy that is caused by converted waves that our acoustic code cannot properly handle. The small change in residual energy between the sixth and tenth iterations indicates that the inversion is nearing convergence. Therefore, we expect very little change in the image after 6 iterations.

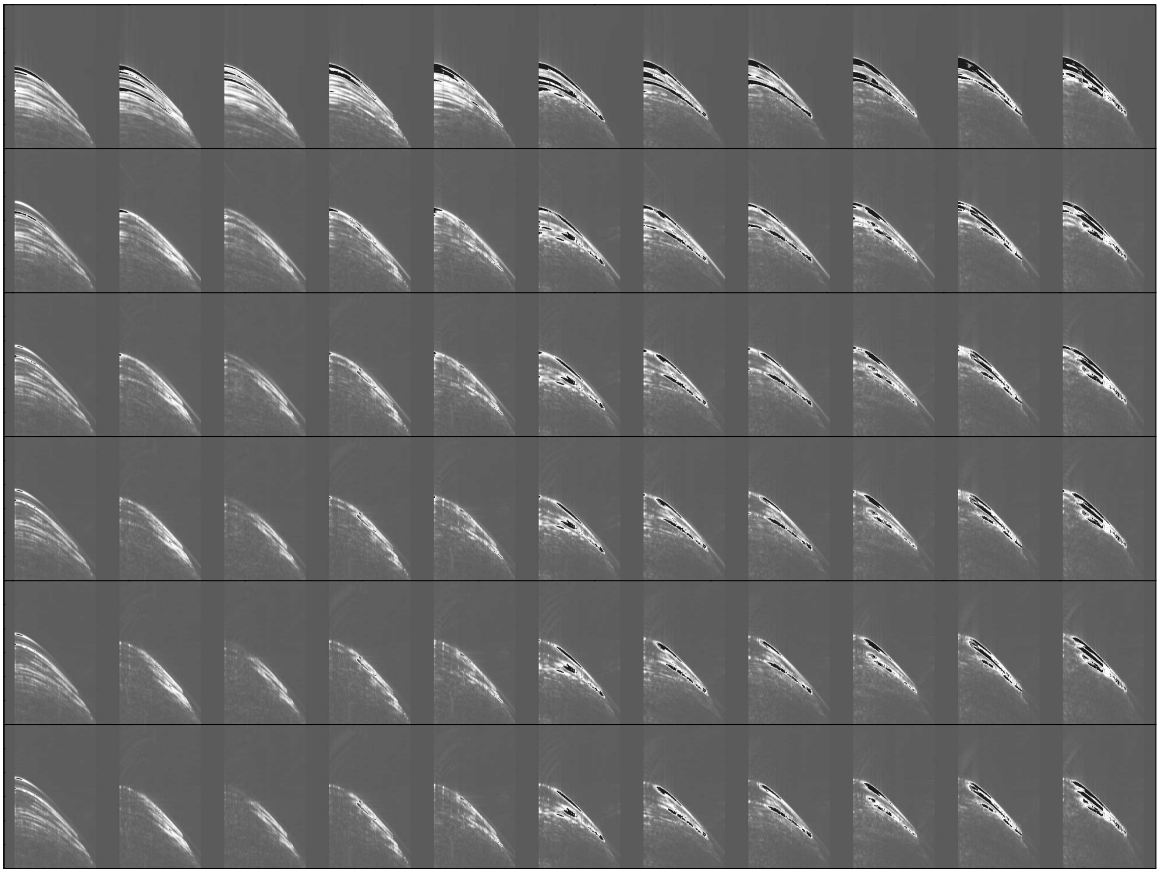

Figure 5: Comparison of the data space residuals from RIP with geophysical regularization. The vertical axis is time, the horizontal axis is offset. Each row is a collection of CMP gathers taken from locations across the whole survey, taking the envelope of the energy and clipping the high values (indicated by black). The first row is the original data, the second row shows the same CMP gathers after 2 iterations, the third row is after 4 iterations, fourth row after 6 iterations, fifth row after 8 iterations and sixth after 10 iterations. marie1-comp.resid [CR,M]

## 3-D RESULTS

To apply RIP to 3-D data, we chose to change our migration operator from downward-continuation migration to common azimuth migration (Biondi and Palacharla, 1996). This helps to keep our computational needs relatively low for a 3-D imaging problem. It also means that we will only be handling the inline offsets, so geophysical RIP will only be acting along the inline offset ray parameter.

### Comparison of 3-D stacked results

The stack of the common azimuth migration (CAM) result (upper panels of Figures 6 and 7) of this 3-D cube is good, indicating that the velocity model is fairly accurate. There are 3-D faults visible away from the salt. Under the salt, the shadow zones caused by poor illumination are easy to identify, although they are full of noise and artifacts.

We performed 7 iterations of 3-D geophysical RIP. The result of the stack can be seen in the lower panels of Figure 6 and Figure 7. The two figures display different inline, crossline, and depth slices, but the types of improvements are the same. In both figures, ovals on the stacked migration result and the stacked geophysical RIP result indicate particular areas where RIP has improved the image. In Fig. 6, oval “A” indicates reflectors that can be followed under the salt nose after imaging with RIP. Ovals “B”, “C”, and “D” show areas on the inline section where the reflectors can be traced almost entirely through the shadow zones after RIP. In the crossline section, many more reflectors are seen after RIP, particularly in oval “E”. In Fig. 7, ovals “A”,“B”, and “C” show areas on the inline section where the reflectors can be traced almost entirely through the shadow zones after RIP and oval “D” shows reflectors and a possible fault in the crossline section.

It is not surprising that the comparison of the migration stack and the RIP stack show less impressive improvements than seen in the 2-D example. Performing only 7 iterations of geophysical RIP, which is regularizing only the inline $p_h$ axis, will not change the image enough to show very significant effects in the stacked volumes. Although there were more substantial improvements in the stacks after 6 iterations of RIP on a 2-D line taken from this dataset (Fig. 4), inverting a 3-D problem means that it can take many more iterations to get similar improvements. However, 3-D RIP does result in clear improvements over the migration results.

### Comparison of unstacked inline results

Using CAM as the imaging operator in our least-squares inversion means that our geophysical regularization operator will only be acting along the inline $p_h$ axis. Therefore, the most significant changes between the CAM result and the geophysical RIP result will be seen in unstacked results. To study these, we have selected several unstacked inline volumes from crossline=20.9 km. These volumes can be seen in Figures 8 through 15, where (if you rotate the pages $90^o$ counter-clockwise) we are displaying the depth slice on the top of the figure,

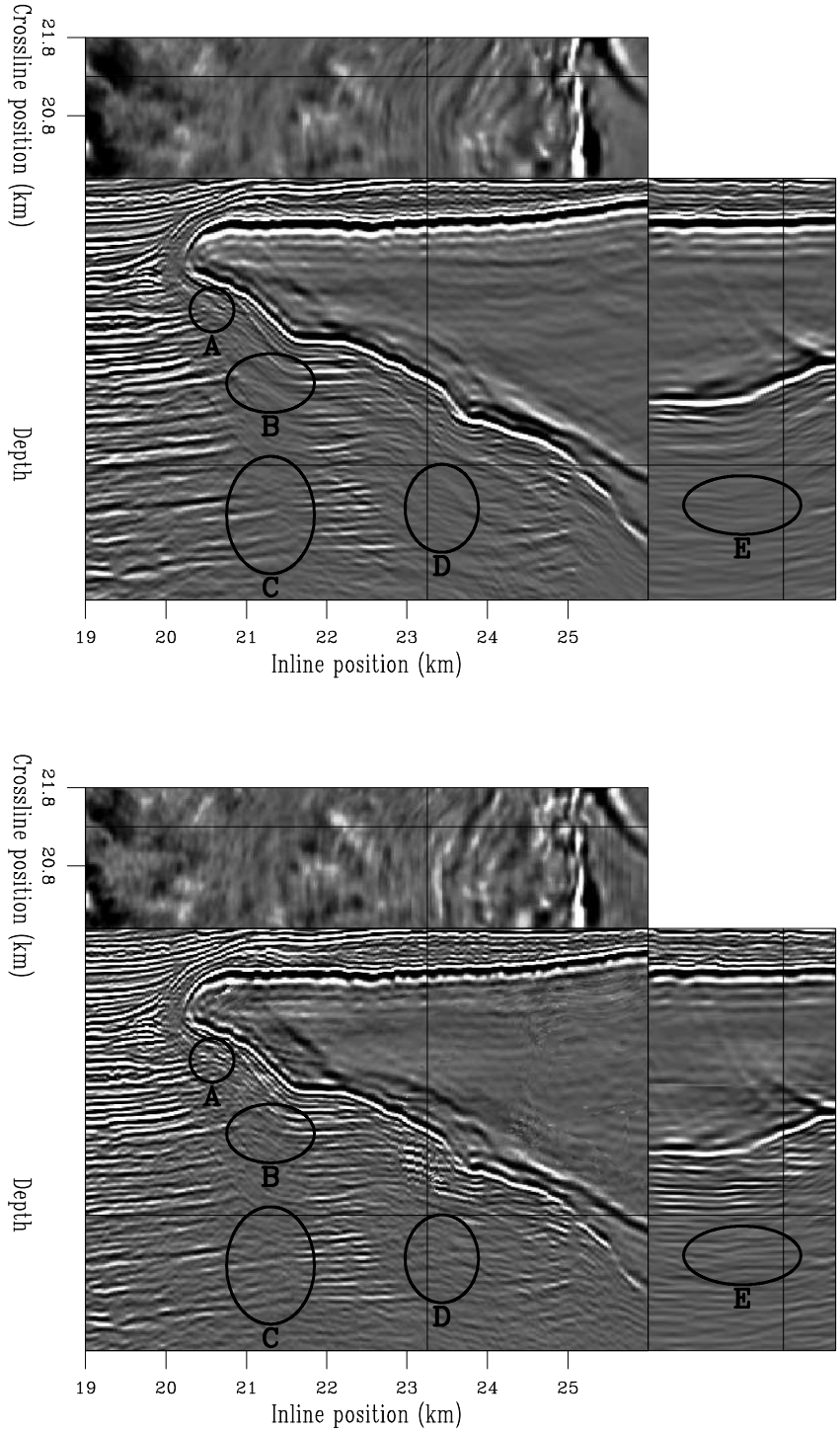


Figure 6: Zoomed 3-D image displayed with depth slice, inline section from crossline=21.3 km and crossline section from inline=23.25 km. Top: stack after common azimuth migration. Bottom: stack after 7 iterations of geophysical RIP. Ovals indicate areas of particular improvement in the RIP result. marie1-zstack3d.1 [CR,M]

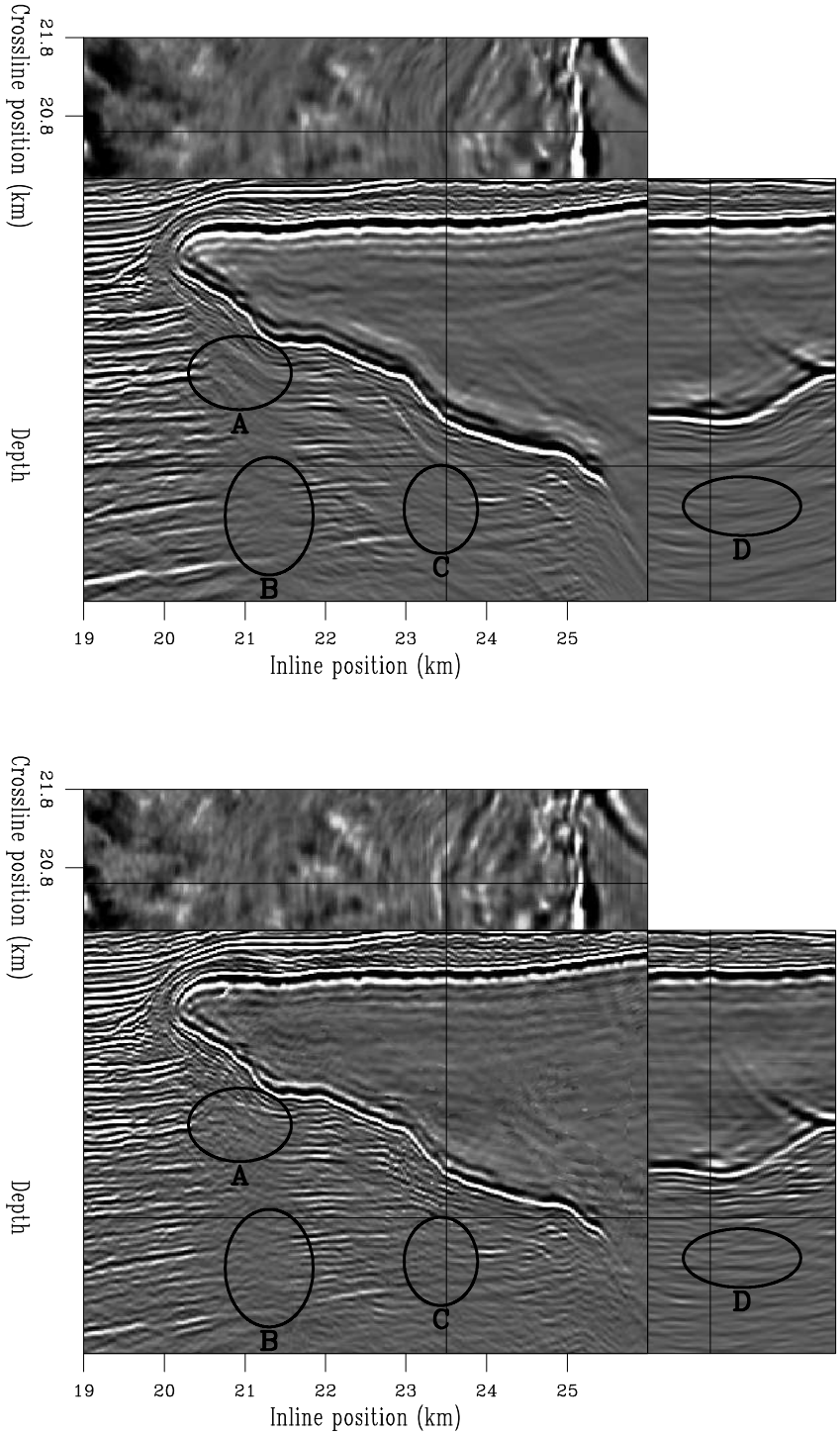


Figure 7: Zoomed 3-D image displayed with depth slice, inline section from crossline=20.6 km and crossline section from inline=23.5 km. Top: stack after common azimuth migration. Bottom: stack after 7 iterations of geophysical RIP. Ovals indicate areas of particular improvement in the RIP result. marie1-zstack3d.2 [CR,M]

the common inline $p_h$ section on the left, and the common image gather to the right of the common inline $p_h$ section. The migration result is shown first, then the geophysical RIP result for each (common inline $p_h$ section - common image gather) pair.

Figures 8 and 9 show a common inline $p_h$ section from $p_h = .1875$ and a common image gather from inline position 20.375 km. Comparing Figure 8 and Figure 9, the RIP result is considerably cleaner. The effects of the regularization are clear in the common image gather (right part of the figures), where the unlabeled oval indicates gaps in the events that are filled by RIP. In the common inline $p_h$ section, the ovals indicate particular areas of the shadow zones that are being filled in. Oval "A" highlights a reflector that, in the migration result, is discontinuous and has inconsistent amplitudes where it does exist. In the RIP result, this reflector is continuous with strong amplitudes along its full extent. Oval "B" extends across one of the shadow zones. The shadow zone is considerably cleaner in the RIP result, with almost none of the up-sweeping artifacts seen in the migration result. Also, the reflectors themselves extend farther into the shadow zone, particularly on the right side of the oval. The events also extend farther into the shadow zone indicated by oval "C".

Moving further under the salt and to a larger offset ray parameter, Figures 10 and 11 show a common inline $p_h$ section from $p_h = .2325$ and a common image gather from inline position 21.65 km. The unlabeled oval in the common image gather shows events that have been strengthen and are more horizontal in the RIP result (Fig. 11) than the migration result (Fig. 10). The ovals marked "A", "B", and "C" on the common $p_h$ sections show the same type of improvement seen in the previous comparison (Figs. 8 and 9). The reflectors at the right side of oval "B" in Figure 11 extend much farther into the shadow zone than those from the migration result.

Another interesting comparison can be made at common inline $p_h$ section from $p_h = .15$ and a common image gather from inline position 20.9 km (Figures 12 and 13). In this migration result (Fig. 12), the common image gather once again has events with gaps caused by poor illumination, indicated by the unlabeled oval. These gaps are largely filled by 7 iterations of RIP, as seen in Figure 13. We see the same improvements in ovals "A", "B", and "C" as discussed for the previous two comparisons. In this comparison, there is an additional oval "D" that indicated reflectors under the salt that are less affected by artifacts and more likely to be accurate in the RIP result than in the migration result.

Finally, looking at the same common image gather from inline position 20.9 km but moving the common inline $p_h$ section to $p_h = .2925$, we compare Figures 14 and 15. In this common $p_h$ section, the effect of a critical angle mute applied during the inversion process can be seen in and below the salt body. The oval in the common image gather shows the same events with gaps in the migration result (Fig. 14) that are filled by RIP (Fig. 15) that was seen in the previous comparison. It is interesting to see that the improvements seen in the "A", "B", and "C" ovals in the previous examples are also seen in this example, at a much larger $p_h$. Obviously, RIP has a positive effect for a large range of $p_h$.

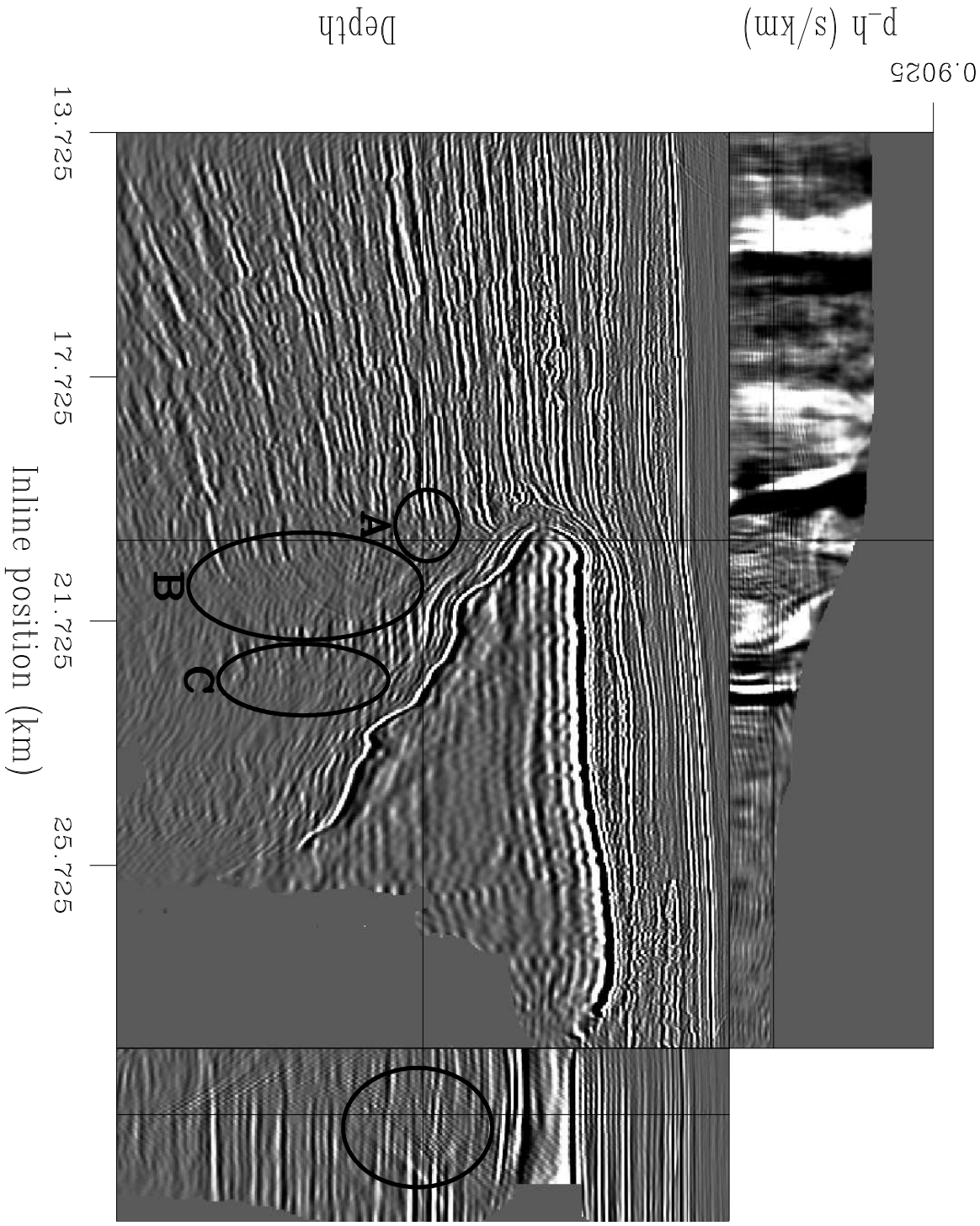


Figure 8: Migration result. Crossline=20.9 km, common inline $p_h$ section from $p_h =$ .1875, and common image gather from inline=20.375 km. Compare with Figure 9. marie1-bp3d.mig.1 [CR]

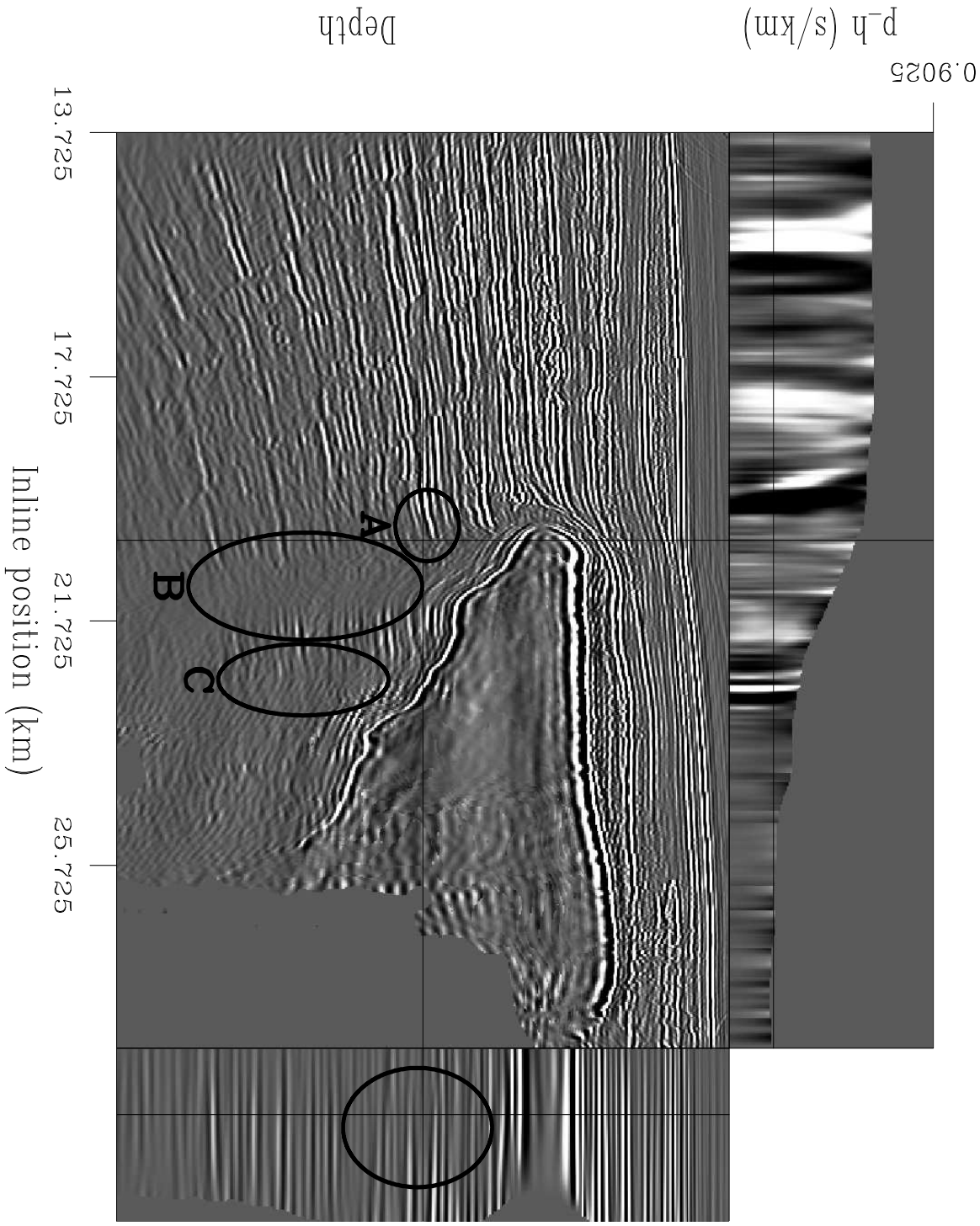


Figure 9: Geophysical RIP result. Crossline=20.9 km, common inline $p_h$ section from $p_h = .1875$, and common image gather from inline=20.375 km. Compare with Figure 8. marie1-bp3d.geop.1 [CR]

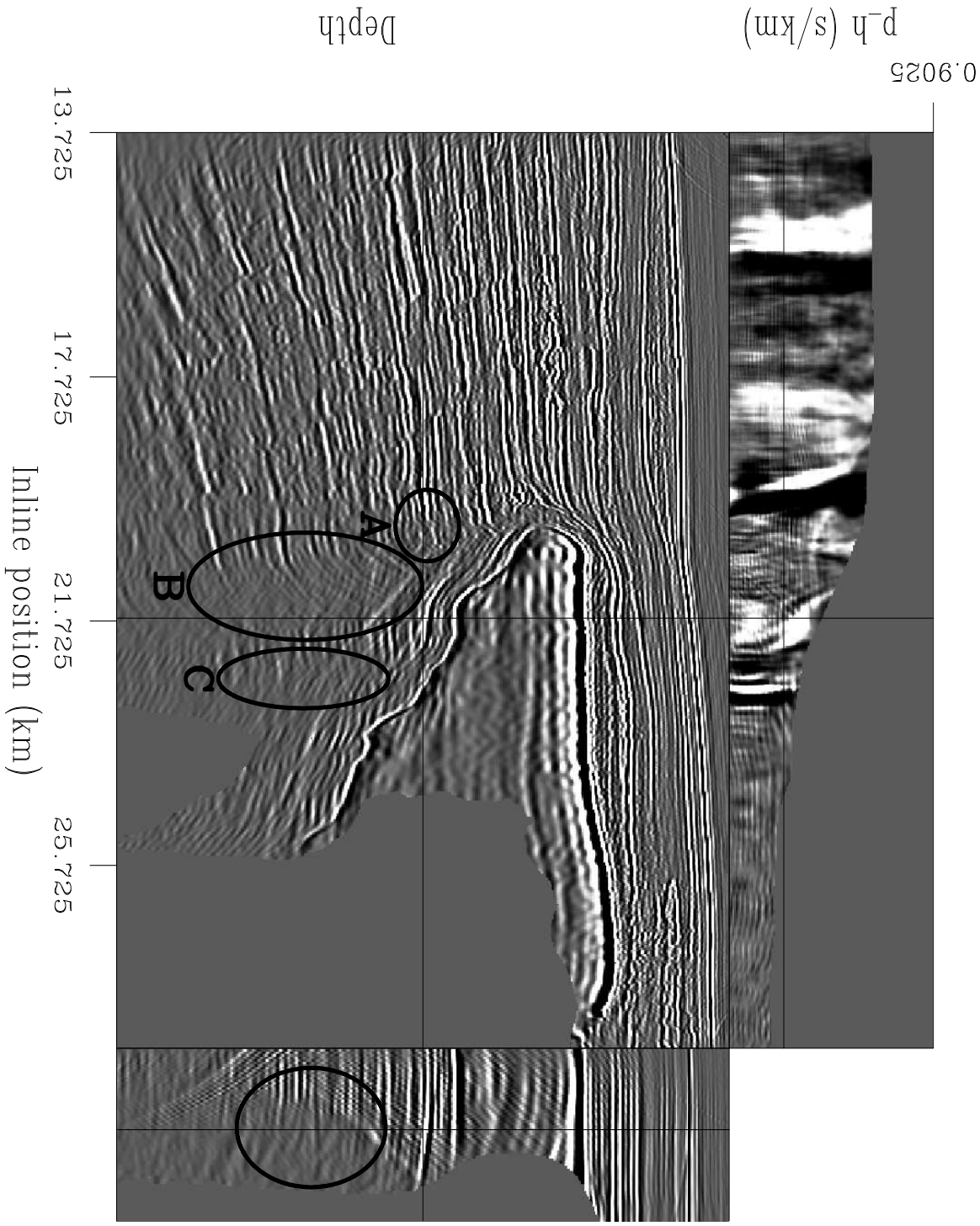


Figure 10: Migration result. Crossline=20.9 km, common inline $p_h$ section from $p_h =$ .2325, and common image gather from inline=21.65 km. Compare with Figure 11. marie1-bp3d.mig.2 [CR]

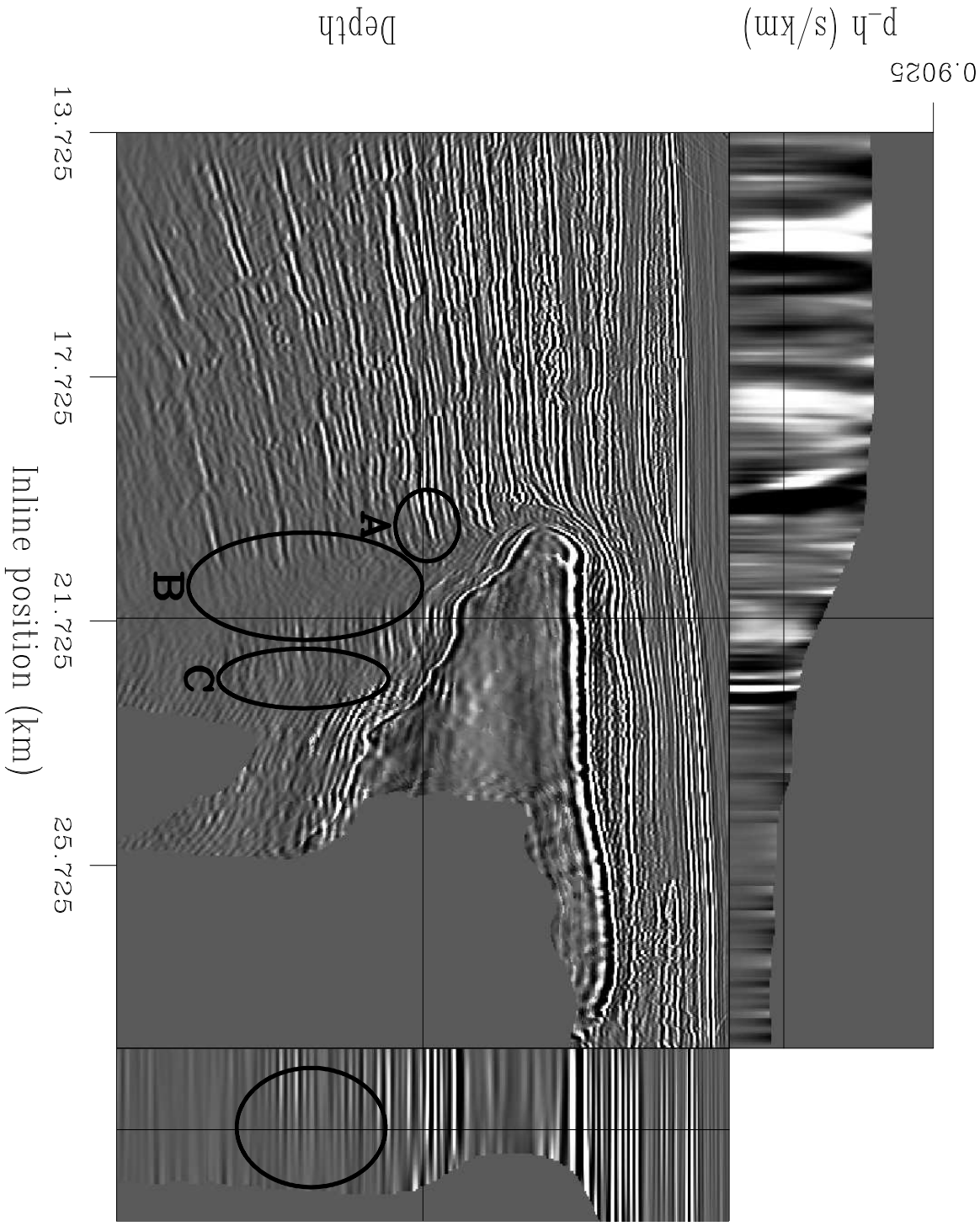


Figure 11: Geophysical RIP result. Crossline=20.9 km, common inline $p_h$ section from $p_h = .2325$, and common image gather from inline=21.65 km. Compare with Figure 10. marie1-bp3d.geop.2 [CR]

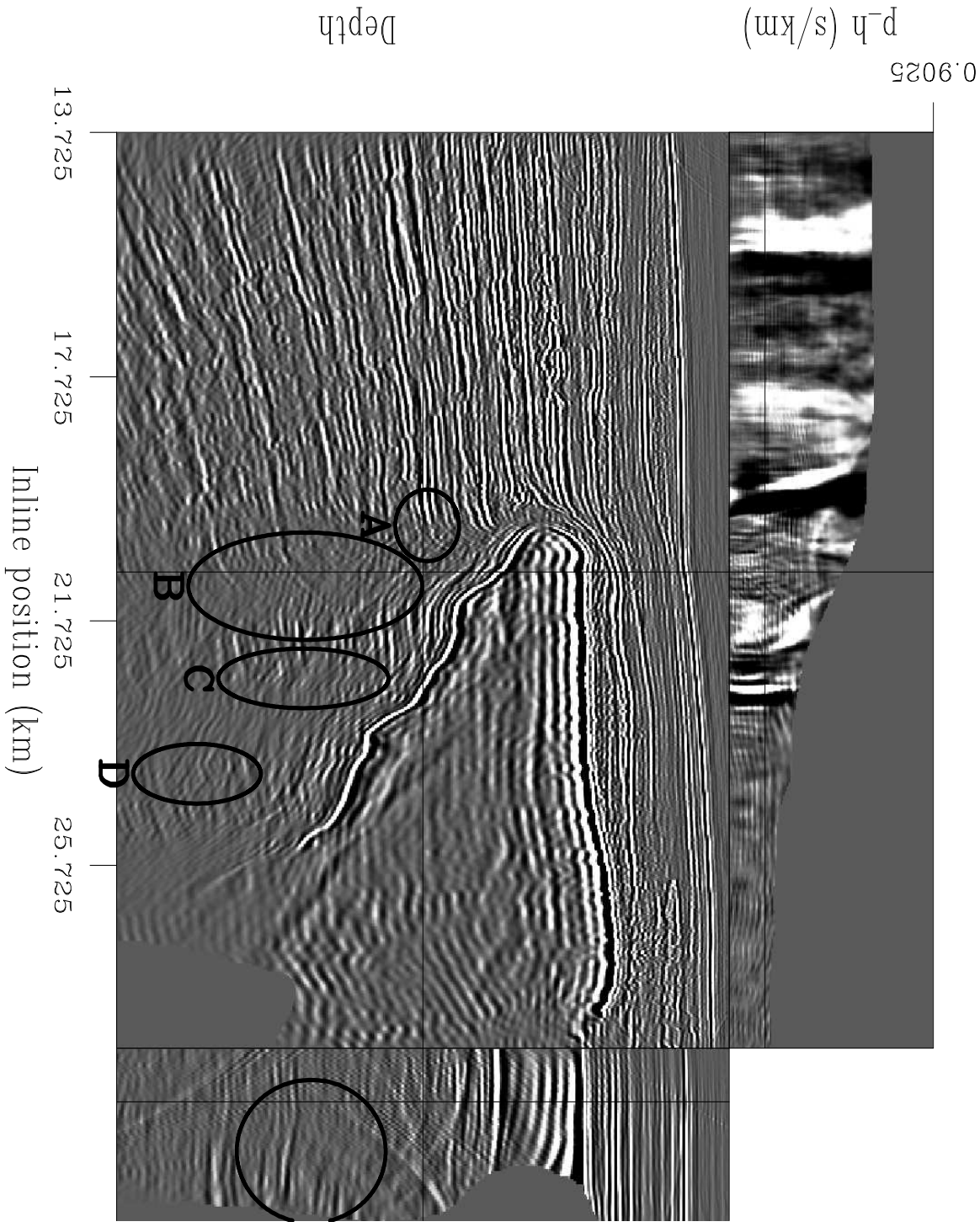


Figure 12: Migration result. Crossline=20.9 km, common inline $p_h$ section from $p_h = .15$, and common image gather from inline=20.9 km. Compare with Figure 13. marie1-bp3d.mig.3 [CR]

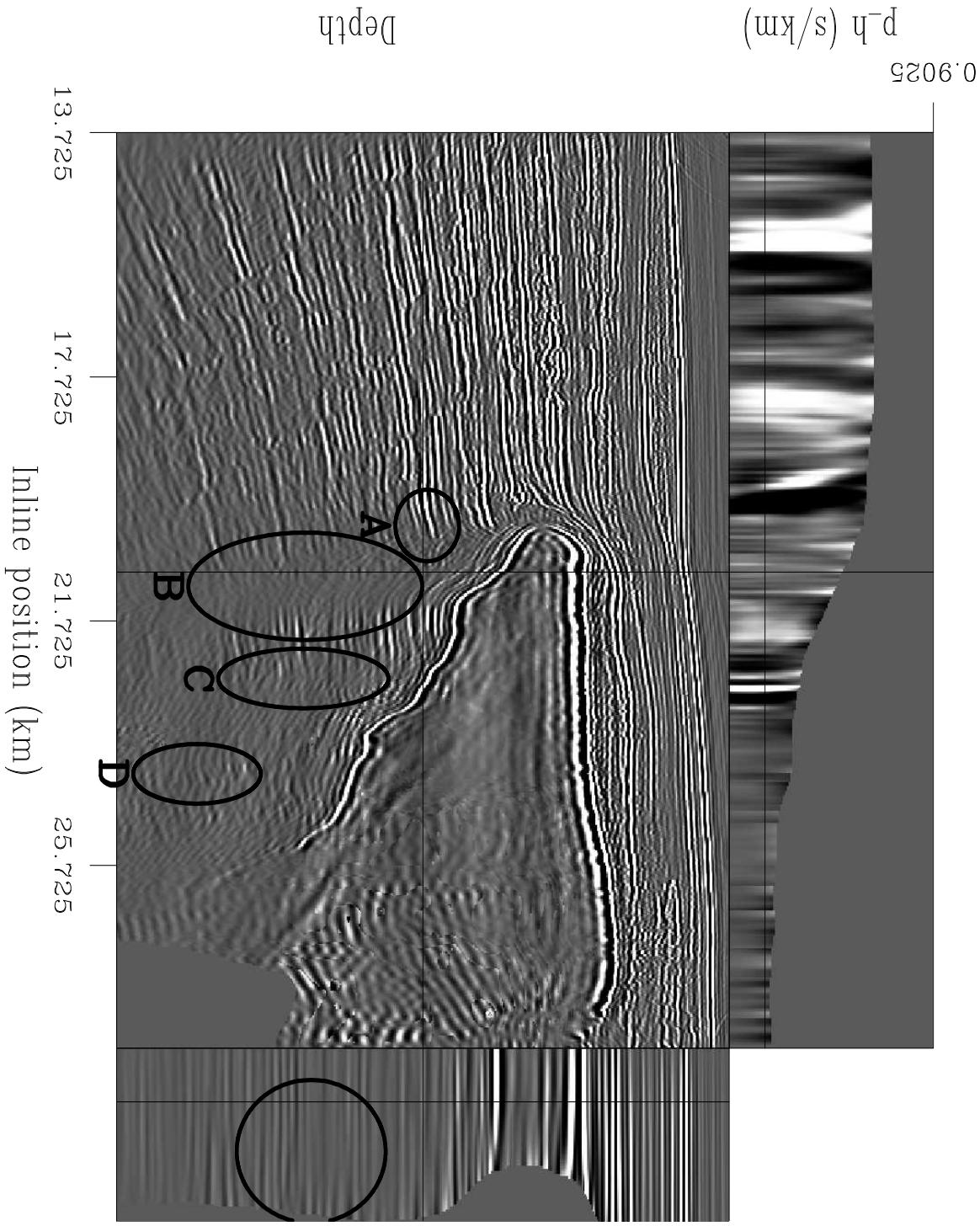


Figure 13: Geophysical RIP result. Crossline=20.9 km, common inline $p_h$ section from $p_h = .15$, and common image gather from inline= 20.9 km. Compare with Figure 12. marie1-bp3d.geop.3 [CR]

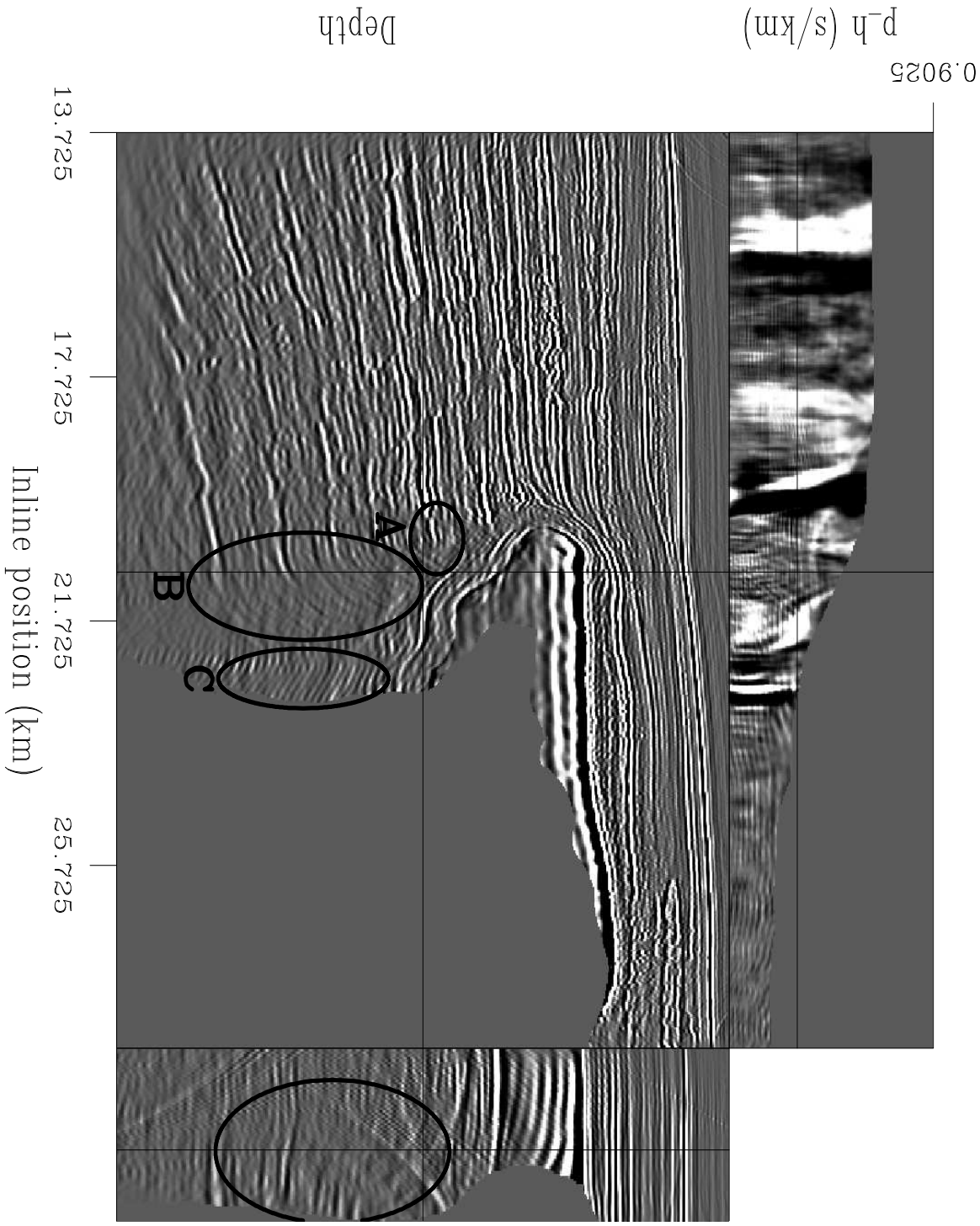


Figure 14: Migration result. Crossline=20.9 km, common inline $p_h$ section from $p_h =$ .2925, and common image gather from inline=20.9 km. Compare with Figure 15. marie1-bp3d.mig.4 [CR]

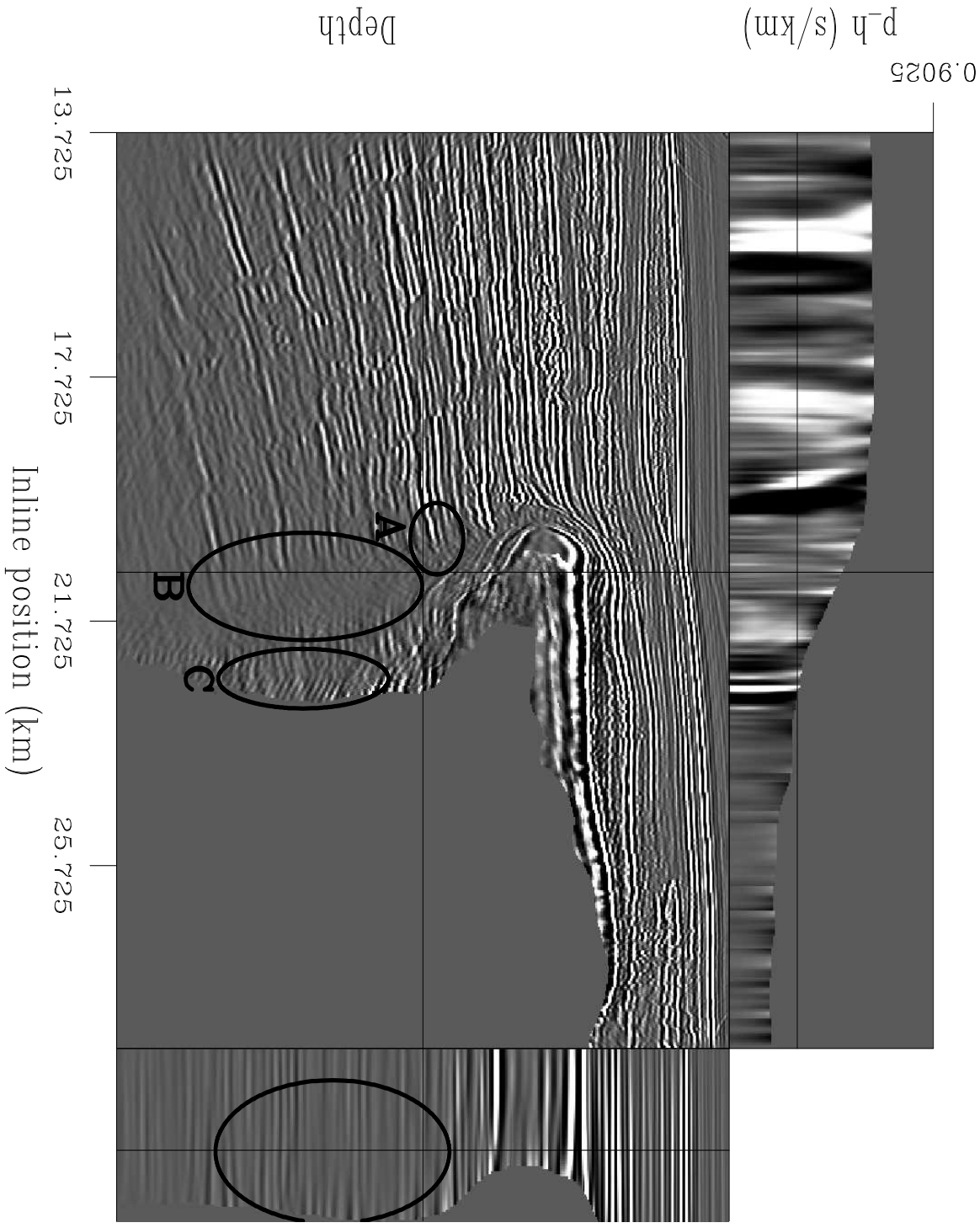


Figure 15: Geophysical RIP result. Crossline=20.9 km, common inline $p_h$ section from $p_h = .2925$, and common image gather from inline=20.9 km. Compare with Figure 14. marie1-bp3d.geop.4 [CR]

## SUMMARY

We have demonstrated the use of regularized inversion with model preconditioning (RIP) with two different imaging operators (downward-continuation migration and common azimuth migration) and a geophysical regularization operator (regularization along the offset ray parameter axis). RIP was applied to a real 2-D line and the 3-D volume that the 2-D line was taken from. In both the 2-D and 3-D cases, RIP was able to improve the resulting image, cleaning up artifacts and increasing the continuity of reflectors through shadow zones caused by poor illumination.

## ACKNOWLEDGMENTS

We would like to thank BP and ExxonMobil, particularly Frederic Billette and John Etgen, for providing us with the Gulf of Mexico dataset.

## REFERENCES

Biondi, B., and Palacharla, G., 1996, 3-d prestack migration of common-azimuth data: Geophysics, **61**, no. 06, 1822–1832.

Claerbout, J., 1998, Multidimensional recursive filters via a helix: Geophysics, **63**, no. 05, 1532–1541.

Clapp, M. L., 2003, Velocity sensitivity of subsalt imaging through regularized inversion: SEP–**114**, 57–66.

Duquet, B., and Marfurt, K. J., 1999, Filtering coherent noise during prestack depth migration: Geophysics, **64**, no. 4, 1054–1066.

Fomel, S., and Claerbout, J., 2003, Multidimensional recursive filter preconditioning in geophysical estimation problems: Geophysics, **68**, no. 2, 577–588.

Fomel, S., Clapp, R., and Claerbout, J., 1997, Missing data interpolation by recursive filter preconditioning: SEP–**95**, 15–25.

Kuehl, H., and Sacchi, M., 2001, Generalized least-squares dsr migration using a common angle imaging condition: 71st Ann. Internat. Meeting, Soc. Expl. Geophysics, Expanded Abstracts, 1025–1028.

Muerdter, D. R., Lindsay, R. O., and Ratcliff, D. W., 1996, Imaging under the edges of salt sheets: a raytracing study: Soc. Expl. Geophys., 66th Annual Internat. Mtg., Soc. Expl. Geophys., Expanded Abstracts, 578–580.

Nemeth, T., Wu, C., and Schuster, G. T., 1999, Least-squares migration of incomplete reflection data: Geophysics, **64**, no. 1, 208–221.

Prucha, M., and Biondi, B., 2002, Subsalt event regularization with steering filters: 72th Ann. Internat. Meeting, Soc. Expl. Geophysics, Expanded Abstracts, 824–827.

Prucha, M. L., Clapp, R. G., and Biondi, B. L., 1998, Imaging under the edges of salt bodies: Analysis of an Elf North Sea dataset: SEP–**97**, 35–44.

Prucha, M., Biondi, B., and Symes, W., 1999a, Angle-domain common image gathers by wave-equation migration: 69th Ann. Internat. Meeting, Soc. Expl. Geophysics, Expanded Abstracts, 824–827.

Prucha, M. L., Biondi, B. L., and Symes, W. W., 1999b, Angle-domain common image gathers by wave-equation migration: SEP–**100**, 101–112.

Ronen, S., and Liner, C. L., 2000, Least-squares DMO and migration: Geophysics, **65**, no. 5, 1364–1371.

Stolk, C., and Symes, W., 2004, Kinematic artifacts in prestack depth migration: Geophysics, **69**, no. 2, 562–575.

Tikhonov, A. N., and Arsenin, V. Y., 1977, Solution of ill-posed problems: John Wiley and Sons.

Xu, S., Chauris, H., Lambare, G., and Noble, M., 2001, Common angle image gather - A strategy for imaging complex media: Geophysics, **66**, no. 6, 1877–1894.